

Infrared Spectroscopy of Matrix-Isolated Polycyclic Aromatic Hydrocarbon Cations. 2. The Members of the Thermodynamically Most Favorable Series through Coronene

D. M. Hudgins[†] and L. J. Allamandola*

NASA Ames Research Center, MS 245-6, Moffett Field, California 94035

Received: August 30, 1994; In Final Form: November 21, 1994[®]

NASA-CR-205316

Gaseous, ionized polycyclic aromatic hydrocarbons (PAHs) are thought to be responsible for a very common family of interstellar infrared emission bands. Here the near- and mid-infrared spectra of the cations of the five most thermodynamically favored PAHs up to coronene: phenanthrene, pyrene, benzo[*e*]pyrene, benzo[*ghi*]perylene, and coronene, are presented to test this hypothesis. For those molecules that have been studied previously (pyrene, pyrene-*d*₁₀, and coronene), band positions and relative intensities are in agreement. In all of these cases we report additional features. Absolute integrated absorbance values are given for the phenanthrene, perdeuteriophenanthrene, pyrene, benzo[*ghi*]perylene, and coronene cations. With the exception of coronene, the cation bands corresponding to the CC modes are typically 2–5 times more intense than those of the CH out-of-plane bending vibrations. For the cations, the CC stretching and CH in-plane bending modes give rise to bands that are an order of magnitude stronger than those of the neutral species, and the CH out-of-plane bends produce bands that are 5–20 times weaker than those of the neutral species. This behavior is similar to that found in most other PAH cations studied to date. The astronomical implications of these PAH cation spectra are also discussed.

I. Introduction

Polycyclic aromatic hydrocarbons (PAHs) form an important class of organic molecules, having long been known to play prominent roles as environmental toxins,¹ and in soot formation.² During the past decade, evidence has been mounting that they are important components of the interstellar medium as well.³ Under the harsh conditions of many interstellar environments, PAHs are expected to be predominantly ionized. For this reason we have undertaken a study of the infrared spectroscopic properties of matrix-isolated PAH cations. While the primary goal of this research is to investigate the role of PAHs in the interstellar medium, the results are of general interest. PAH cations are considered to be important intermediates in combustion,² and PAH intermediates and primary reaction products are directly related to the carcinogenicity of some members of this hydrocarbon family.¹

Ionized⁴ and neutral⁵ PAH molecules have been proposed as the carriers of a very common family of interstellar infrared fluorescence bands at 3050, 1615, 1310, 1150, and 885 cm⁻¹ (3.3, 6.2, 7.7, 8.7, and 11.3 μm). The ubiquity of this spectrum suggests that free molecular PAHs are common throughout interstellar space, and the intensity of the bands indicates that they are as abundant as the most abundant polyatomic interstellar molecules known. As much as 30–40% of the radiant energy from some of these sources is emitted in this family of bands. Reviews of this field can be found in ref 3.

While the interstellar PAH hypothesis rests on the general resemblance of the interstellar emission spectra to the absorption spectra of aromatic hydrocarbons, the available data are mainly for neutral PAHs suspended in salt pellets⁶ or organic solvents.⁷ Under such conditions, interactions with the surrounding medium and with other PAH molecules (clusters) strongly perturb the transitions.⁸ While this body of information has

been invaluable in establishing the interstellar PAH hypothesis, there are important differences in details between the laboratory and interstellar spectra. Differences in band position and relative band intensities, as well as the fact that most interstellar PAHs are expected to be isolated and ionized in the regions where they emit, have hindered the verification of the hypothesis and the exploitation of PAHs as probes of the interstellar medium. Thus, the infrared spectra of neutral, isolated PAHs and of ionized, isolated PAHs are of fundamental importance to further progress in this field.

There has been substantial progress recently in experimentally measuring the emission spectra of vibrationally excited, gas phase aromatic molecules. Elegant UV-pumped IR emission experiments on gas phase neutral PAHs have been carried out.^{9–13} The results of these experiments, in conjunction with absorption studies of PAHs in the gaseous state at various temperatures,^{14–18} show that (i) the emission peak frequency of the aromatic CH stretch in gas phase PAHs shifts as a function of internal energy content and matches that of the interstellar band at 3050 cm⁻¹ at reasonable levels of excitation; (ii) the bandwidth increases with energy and matches that of the interstellar band at similarly appropriate internal energies; and (iii) the plateau that underlies the interstellar feature, and extends out to about 2740 cm⁻¹, is reproduced as well. Schlemmer et al.,¹² in reporting the gas phase emission from naphthalene and pyrene, show that the relative intensities of the emission bands differ in absorption from those for the same species and from the relative intensities of the interstellar emission features. Thus, they conclude that small neutral PAHs cannot be the carriers of the interstellar bands. This is, of course, consistent with PAHs being ionized in the emission zones. These emission experiments on neutral PAHs are inherently very difficult, and it will likely be some time before this type of measurement will be carried out on ionized PAHs. These results raise important, fundamental questions regarding the molecular physics of the infrared emission process from vibrationally excited molecules.

* Author to whom correspondence should be addressed.

[†] Current address: Department of Chemistry, Adrian College, Adrian, MI 49221.

[®] Abstract published in *Advance ACS Abstracts*, February 1, 1995.

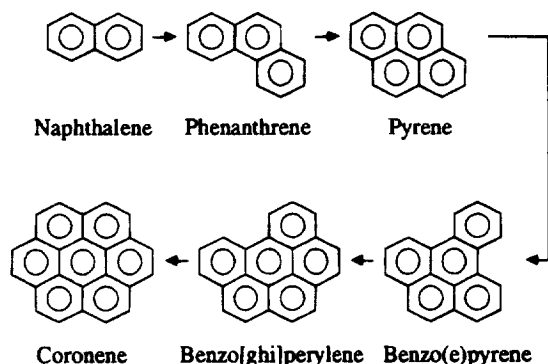


Figure 1. First six members of the most thermodynamically favorable, high-temperature PAH polymerization route, adapted from Stein.²⁰ Successive members of this series are formed by adding two or four carbon atoms at a time, the number required to complete an additional fused aromatic ring. Note that the C₂ and C₄H₂ groups needed to go from one species to the next refer only to the number and type of atoms added in each step and do not refer to specific chemical species or mechanisms. Similarly, the circles here indicate planarity and overall electron delocalization, not superaromaticity.

There is also a need for reliable, quantitative infrared absorption data on neutral and ionized PAHs at the low temperatures characteristic of the interstellar medium. We have initiated a systematic program to obtain this information. In the first paper in this series, we reported our experimental approach to the problem and presented results from 4000 to 200 cm⁻¹ on the smallest PAH, naphthalene (C₁₀H₈), and its fully deuterated analog, (C₁₀D₈).¹⁹ We now have the infrared spectra for a number of neutral PAHs and their cations. Here the spectroscopic properties of the members of the thermodynamically most favored PAH species containing between 6 and 24 carbon atoms are presented. Stein and co-workers²⁰ have extensively investigated the thermodynamic properties of aromatic species, showing that, of the hundreds of PAH isomers possible in this size range, those in Figure 1 are thermodynamically most favored under high-temperature PAH growth conditions. Thus, these are likely to be important in the circumstellar environments in which PAHs are produced and able to survive the harsh conditions of many of the interstellar emission regions. In subsequent papers in this series, different aspects of PAH cation structure, including tetracyclic PAHs, polyacenes, and PAHs incorporating 5-membered rings, will be explored. The neutral spectra of these PAHs will be presented elsewhere.^{21,22} Our motivation is to understand how structure and size influence the infrared spectra of small PAHs in their neutral and cationic forms.

Efforts to provide this type of information are also underway at several other institutions. Defrees and Miller carried out theoretical calculations on the expected infrared spectral properties of the naphthalene and anthracene cations and predicted surprising relative band strength differences between the neutral and ionized forms of these PAHs.^{23a} Subsequently, Defrees et al.^{13b} and Pauzat et al.²⁴ have greatly expanded this work. Professor Vala and co-workers at the University of Florida have published the infrared spectroscopic properties for cations of the PAHs naphthalene, anthracene, pyrene, perylene, and coronene,²⁵⁻²⁸ and d'Hendecourt et al. have reported the spectrum of the coronene cation.²⁹

This paper is laid out as follows. The experimental techniques are summarized in section II. In section III are presented the near- and mid-infrared spectra of the phenanthrene, phenanthrene-*d*₁₀, pyrene, pyrene-*d*₁₀, benzo[*e*]pyrene, benzo[*ghi*]perylene, and coronene cations. These results are discussed in

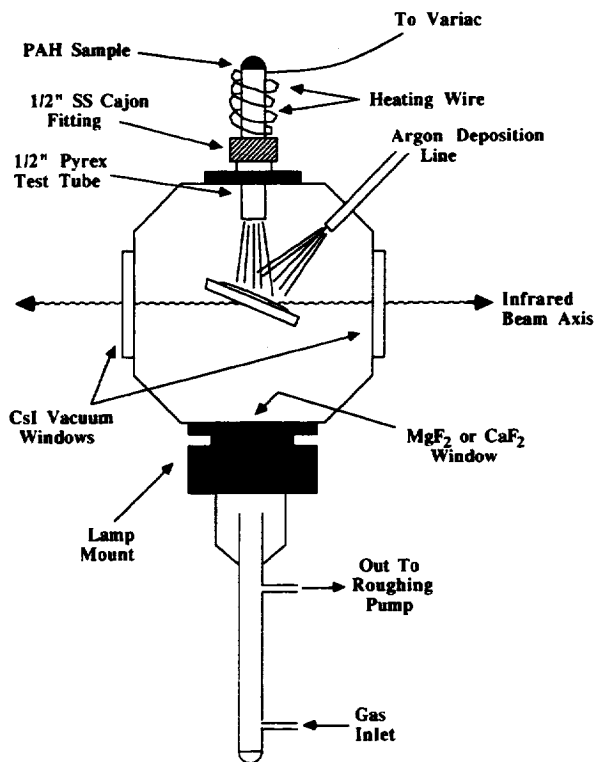


Figure 2. Schematic cross section of the matrix isolation sample chamber.

section IV, where trends and implications regarding the interstellar question are pointed out.

II. Experimental Section

The matrix isolation technique is employed to isolate individual polycyclic aromatic hydrocarbon (PAH) molecules in an argon matrix, where they are photoionized and probed spectroscopically. Argon matrices are known to be suitable for vibrational studies, typically causing small shifts in the 0–15 cm⁻¹ range. For electronic transitions, a neon matrix is required to avoid serious perturbations. With the exception of the sample deposition procedure, our experimental procedure has been described in detail previously.¹⁹ A schematic cross section of the sample chamber is shown in Figure 2. Briefly, an infrared-transmitting substrate (CsI) is suspended inside an ultra-high vacuum chamber and cooled by a closed-cycle helium refrigerator. The ultra-high vacuum chamber ($p \sim 10^{-8}$ mTorr) is equipped with multiple inlet ports, and the cooler is mounted in such a way that the infrared window can be rotated to face any of these ports without breaking the vacuum. Typically, the CsI window was cooled to 10 K and positioned to face the sample deposition inlets. Samples were prepared by co-deposition of a gaseous PAH with a large overabundance of argon to a thickness appropriate for generation of the cation and measurement of its infrared spectrum. After sample deposition was complete, the cold head was rotated to face the beam of an infrared spectrometer so that a prephotolysis spectrum could be recorded. The sample was then rotated to face a vacuum ultraviolet lamp for photolysis. The sample was finally returned to the scanning position where the postphotolysis spectrum was recorded. Comparison of this spectrum with the neutral spectrum permitted identification of the ion features that appeared upon photolysis.

A. Sample Preparation. PAHs containing three or more rings do not have sufficient vapor pressure at room temperature to permit their preparation as a gaseous mixture with argon, as

was the case in our previous study involving naphthalene. This necessitated the vaporization of the PAH of interest and subsequent co-deposition of the gaseous PAH molecules with excess argon. To this end, PAH samples were placed in resistively heated Pyrex tubes ($1/2$ in. diameter) and mounted on the sample chamber through a stainless steel Cajon Ultra-torr fitting. The temperature of the PAH was monitored using a chromel/alumel thermocouple mounted on the exterior of the tube with aluminum tape. Such an arrangement should potentially be useful at temperatures as high as $316\text{ }^{\circ}\text{C}$ (the failure temperature of the Viton O-ring) and with samples as small as a few milligrams. Argon was admitted through a second port at a position 45° from the first in such a way that the two streams coalesced before the surface of the cold window. The deposition tubes ended between 2 and 4 cm from the cold window. During deposition, this window was maintained at a position intermediate between the two deposition ports (Figure 2). The argon deposition line was liquid nitrogen trapped to minimize contamination.

Sample quality was found to be optimal for PAH vapor pressures in the range 10–30 mTorr. Higher vapor pressures required higher argon deposition rates that exceeded the thermal conductivity of the CsI window, warming the matrix. The annealing that resulted produced a matrix that was highly scattering at short wavelengths, crippling the Lyman- α photoionization efficiency and the signal-to-noise ratio of the near-IR spectrum. Conversely, lower vapor pressures required longer deposition times, which necessarily increased the contaminants in the matrix and, in turn, reduced the ionization efficiency. Thermochemical data³⁰ were used to establish the approximate temperature necessary for each PAH investigated. Optimum tube temperatures were as follows: phenanthrene, $10\text{ }^{\circ}\text{C}$; pyrene, $60\text{ }^{\circ}\text{C}$; benzo[e]pyrene, $97\text{ }^{\circ}\text{C}$; benzo[ghi]perylene, $137\text{ }^{\circ}\text{C}$; and coronene, $158\text{ }^{\circ}\text{C}$. The optimal argon flow rate was estimated to be between 0.5 and 1.0 mmol/h.

As was the case in our earlier study of the naphthalene cation,¹⁹ photoionization of PAH/Ar matrices was accomplished using the Lyman- α emission from a microwave-powered discharge lamp optimized by the use of a 10% H_2 in He gas mixture at ~ 75 mTorr. A MgF_2 vacuum window allowed transmission of this radiation to the sample. For those experiments incorporating the electron acceptor CCl_4 in the matrix, lower energy photolysis was necessary. Lyman- α photons (10.35 eV) are sufficiently energetic to ionize matrix-isolated CCl_4 ($\text{IE}_{\text{gas}} = 11.28\text{ eV}$)³¹ molecules, negating their usefulness as electron acceptors. For those experiments, UV radiation was generated by a discharge in pure H_2 gas at ~ 150 mTorr. This optimized the broad molecular hydrogen emission band centered around 160 nm (7.77 eV) with respect to the Lyman- α line. A CaF_2 vacuum window (cutoff $\lambda \approx 150$ nm) served as a filter to exclude the residual Lyman- α radiation.

This technique results in ion yields ranging from 5 to 10%. Specifically, the yields for the spectra presented here were as follows: phenanthrene, $9 \pm 4\%$; phenanthrene- d_{10} , $7 \pm 4\%$; pyrene, $10 \pm 5\%$; benzo[e]pyrene, $6 \pm 3\%$; benzo[ghi]perylene, $10 \pm 5\%$; and coronene, $11 \pm 6\%$. These yields were determined as previously described.¹⁹

Pure argon samples having pressures in the range 75–225 Torr were prepared as described previously.¹⁹

The PAHs used in this investigation include phenanthrene (Aldrich Chemical Co., 98+% purity), phenanthrene- d_{10} (Aldrich, 97% purity), pyrene (Aldrich, 99% purity), pyrene- d_{10} (Cambridge Isotope Laboratories, 98% purity), benzo[e]pyrene (Aldrich, 99% purity), benzo[ghi]perylene (Aldrich, 98% purity), and coronene (Pfaltz and Bauer, Inc., 97% purity). All samples

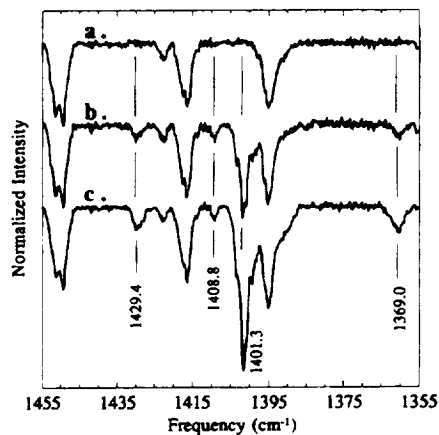


Figure 3. Enhancement of the benzo[ghi]perylene cation yield with the addition of CCl_4 to the matrix. The $1455\text{--}1355\text{ cm}^{-1}$ region of the spectrum of matrix-isolated benzo[ghi]perylene: (a) before photolysis; (b) after 8 min of *in situ* photolysis; (c) after 8 min of *in situ* photolysis of a matrix containing CCl_4 at the level of 1 part in 200.

were used without further purification. Matheson prepurified argon (99.998% minimum) was used in these studies.

B. Spectroscopy. The sample chamber, now equipped with CsI vacuum windows, is suspended in the sample compartment of an FTIR spectrometer (Nicolet Analytical Instruments, Model 740). All spectra reported here were measured at 0.5 cm^{-1} resolution. This resolution is critical in detecting ion bands that fall near the position of a neutral band. Spectra typically were generated through the coaddition of five blocks of 200 scans, a number that optimized both the signal-to-noise ratio and the time requirements of each experiment.

Mid-infrared spectra ($7000\text{--}500\text{ cm}^{-1}$) were collected using an MCT-B detector/KBr beam splitter combination. Near-infrared spectra ($15100\text{--}8800\text{ cm}^{-1}$) were collected using a silicon detector/quartz beam splitter combination. Conversion between the two spectral regions allowed the measurement of both electronic and vibrational band intensities from a single matrix.

C. Cation Band Identification. Three criteria must be satisfied before a photoproduct band is attributed to a particular PAH cation. First, the bands must appear only when the associated neutral PAH is present in the matrix. An extensive number of control experiments have been carried out to ensure that this is the case. Second, the bands attributed to the cation must be markedly enhanced when CCl_4 , an electron acceptor, is present in the matrix at a concentration of 1 part in 200. This behavior establishes that the bands arise from a positive ion. This effect is demonstrated in Figure 3, which shows a portion of the spectrum of the benzo[ghi]perylene cation generated both with and without CCl_4 in the matrix. Third, all the bands attributed to the cation must evolve in a similar fashion. Spectra collected as a function of photolysis time show that all of the bands assigned to the respective cation grow and decline together in a manner distinct from other features produced by photolysis. These band correlation plots are presented on a molecule by molecule basis along with the appropriate spectroscopic data. In general, the intensities of the bands corresponding to the PAH cation (plotted showing data points) peak after 4–8 min of photolysis and then remain essentially constant or fall off slightly upon further photolysis. This behavior is consistent with that observed previously for the naphthalene cation and discussed in ref 19. Conversely, the bands of other photoproducts (plotted without data points shown) tend to increase steadily with photolysis time. Rogue photoproduct bands were not common, typically numbering 2–4 in each case. Most common were

TABLE 1: Infrared Frequencies and Relative Intensities for the Cations of the Most Thermodynamically Favorable PAHs

naphthalene		phenanthrene		pyrene		benzo[e]pyrene		benzo[ghi]perylene		coronene	
ν (cm ⁻¹)	I_{rel}										
758.7	0.27	582.0	0.220	690.1	0.228	685.7	0.150	639.6	0.218	874.5	1.00
1023.2	0.054	694.5	0.0944	861.0	0.270	848.0	0.218	863.6	0.445	1378.6	0.174
1214.9	0.2	756.2	0.0731	867.0	0.0353	873.3	0.131	1216.7	0.0317	1579.0	0.825
1218.0	1.0	836.0	0.0557	953.8	0.0665	1193.9	0.214	1223.4	0.295		
1400.9	0.044	1258.7	0.0414	976.5	0.0904	1264.3	0.138	1311.9	0.134		
1518.8	0.1	1264.7	0.0142	1102.0 ^a	0.0793	1308.2	0.186	1324.4	0.737		
1525.7	0.29	1267.0	0.142	1188.7	0.0364	1336.0	0.806	1331.9	0.168		
		1277.5/1282.5	0.836	1216.0	0.121	1349.2	1.00	1343.2	0.321		
		1299.0	0.0884	1245.1	0.343	1357.0	0.154	1350.2	0.143		
		1513.0	0.0424	1253.7/1255.7	0.0425	1368.2	0.129	1369.0	0.625		
		1551.0	0.0625	1356.1/1358.4	1.00	1410.5	0.407	1401.3	0.833		
		1558.2	0.0211	1361.8	0.158	1435.6	0.0957	1408.8	0.0472		
		1565 complex	1.00	1421.1	0.158	1467.0	0.0969	1429.4	0.0970		
				1440.3	0.101	1556.8	0.878	1538.6	0.0185		
				1550.9/1553.4/1556.0	0.891			1550.1	0.220		
								1578.2	1.00		

^a Due to its low intensity and separation from other features, this band is not shown in Figure 8.

TABLE 2: Comparison of the Infrared Frequencies and Relative Intensities for Isotopomeric Forms of the Cations of Naphthalene, Phenanthrene, and Pyrene

naphthalene				phenanthrene				pyrene			
C ₁₀ H ₈ ⁺		C ₁₀ D ₈ ⁺		C ₁₄ H ₁₀ ⁺		C ₁₄ D ₁₀ ⁺		C ₁₆ H ₁₀ ⁺		C ₁₆ D ₁₀ ⁺	
ν (cm ⁻¹)	I_{rel}	ν (cm ⁻¹)	I_{rel}	ν (cm ⁻¹)	I_{rel}	ν (cm ⁻¹)	I_{rel}	ν (cm ⁻¹)	I_{rel}	ν (cm ⁻¹)	I_{rel}
758.7	0.27	1063.1	0.16	582.0	0.220	566.7	0.101	690.1	0.228	952.5	0.0385
1023.2	0.054	1075.4	1.0	694.5	0.0944	856.2	0.187	861.0	0.270	961.9	0.0783
1214.9	0.2	1077.3	0.068	756.2	0.0731	958.5	0.0183	867.0	0.0353	1288.0	0.720
1218.0	1.0	1373.8	0.14	836.0	0.0557	1013.4 ^a	0.0214	953.8	0.0665	1317.8	0.0882
1400.9	0.044	1379.4	0.10	1258.7	0.0414	1114.8	0.0274	976.5	0.0904	1362.2	1.00
1518.8	0.1	1463.8	0.42	1264.7	0.0142	1176.6	0.0161	1102.0 ^b	0.0793	1366.4	0.00907
1525.7	0.29	1466.2	0.28	1267.0	0.142	1194.1	0.0309	1188.7	0.0364	1391.5	0.463
				1277.5/1282.5	0.836	1201.6	0.349	1216.0	0.121	1511.8	0.889
				1299.0	0.0884	1207.2	0.116	1245.1	0.343	1517.0	0.174
				1513.0	0.0424	1213.5	0.0186	1253.7/1255.7	0.0425	1521.1	0.0824
				1551.0	0.0625	1221.5	0.0530	1356.1/1358.4	1.00	1540.1	0.0532
				1558.2	0.0211	1230.4	0.0721	1361.8	0.158		
				1565.0	1.00	1296.5	0.0336	1421.1	0.158		
						1344.2	0.0234	1440.3	0.101		
						1400.3	0.0309	1550.9/1553.4/1556.0	0.891		
						1459.5	0.189				
						1507.0	0.105				
						1525.0/1528.0	1.00				
						1547.4	0.0485				

^a Due to its low intensity and separation from other features, the C₁₄D₁₀⁺ band at 1013.4 cm⁻¹ is not shown in Figure 6. ^b Due to its low intensity and separation from other features, the C₁₆H₁₀⁺ band at 1102.0 cm⁻¹ is not shown in Figure 8.

the 904 cm⁻¹ (HAr₂⁺) and 1589 cm⁻¹ bands. These appeared moderately strong in a number of experiments. Other weak photoproduct bands at 1388 and 1104 cm⁻¹ (HO₂⁺) and at 1039 cm⁻¹ (O₃) appeared in several experiments, as did bands attributable to CO₂ and possibly CO.

III. Results

There are many PAHs that one can study. Those studied at the NASA Ames Research Center have been selected for the following reasons. First, as little is known about the infrared properties of PAH cations, the smallest members of the PAH family were chosen to minimize the number of fundamental vibrations and spectral complexity. Second, as this work is motivated by the astrophysical question, the PAHs most likely to be important in this context were given first preference. Thus, the thermodynamically most favorable members of the high-temperature PAH formation route containing 6–24 carbon atoms were studied (Figure 1).¹⁹ These spectra are presented here in the second paper of the series. Third, as the effects of structure and size on the infrared spectra of simple PAH cations are not known, related PAHs with limited, well-defined structural

differences have been studied together. Finally, as size increases, PAH samples tend to become increasingly refractory and increasingly difficult and expensive to obtain. Thus, in the interest of experimental practicality, smaller PAHs were the logical starting point. Small PAHs are also relevant from the astrophysical point of view. Indeed, a QRRKM analysis of the interstellar spectra indicates that molecules containing 20–30 carbon atoms dominate the fluorescence at the shortest wavelengths.^{3a,4}

The positions and relative intensities of the mid-infrared cation bands for the thermodynamically most favorable series of PAHs up to coronene are shown in Table 1. In addition, the spectra of the perdeuterated phenanthrene (C₁₄D₁₀⁺) and pyrene (C₁₆D₁₀⁺) cations have also been measured. Band positions and relative intensities are compared with those of the fully hydrogenated cations and with those of naphthalene (C₁₀H₈⁺ and C₁₀D₈⁺) in Table 2. The infrared spectra of the cations of the thermodynamically most favorable series of PAHs are presented in the order of increasing molecular size. Only those regions of the spectrum where cation bands appear are shown. The complete spectra of the neutral isolated PAHs will be given

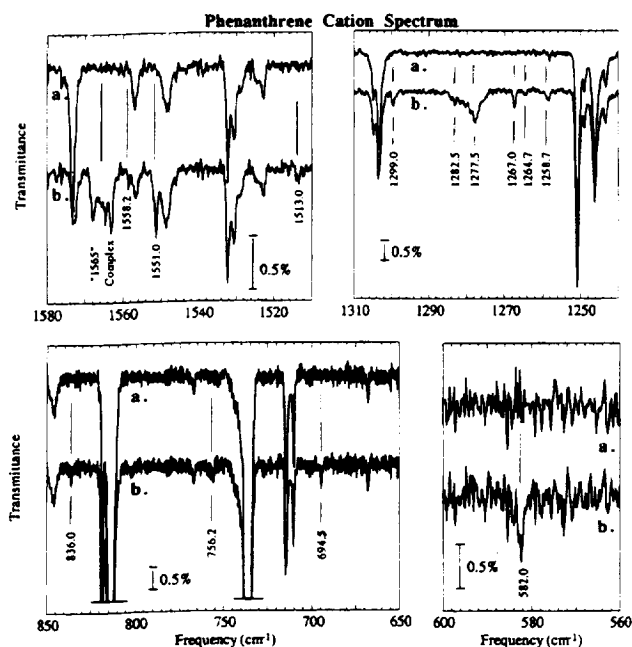


Figure 4. Mid-infrared spectra of the phenanthrene cation isolated in an argon matrix at 10 K: (a) before photolysis; (b) after 8 min of *in situ* photolysis. The cation bands are labeled with their positions.

later.²¹ The spectrum of the naphthalene cation, the first multiring aromatic of the series, has been presented elsewhere.^{19,25} Additional discussions of the pyrene and coronene cations can be found elsewhere.^{27,29}

A. Mid-Infrared Spectroscopy. Screening by the CH stretching bands due to the much more abundant neutral molecules prevents detection of any of the PAH cation bands in the 3200–2900 cm^{-1} region. The difficulty inherent in detecting the infrared active CH stretching modes of the PAH cations studied to date is consistent with theoretical calculations that have predicted that the CH stretching bands of the cation are suppressed relative to the analogous bands of the neutral counterparts.^{23a,b,24}

The Phenanthrene Cation, $\text{C}_{14}\text{H}_{10}^+$. The mid-infrared spectrum of the phenanthrene cation is shown in Figure 4. The band frequencies and relative intensities are listed in Table 1. The evolution of the bands assigned to the cation with Lyman- α photolysis is plotted in Figure 5. This band correlation, one of the criteria of ion assignment, is looser for the weaker bands whose signal-to-noise ratios lie in the 2–3 range. Nonetheless, their overall behavior of a sharp rise and leveling off warrants their assignment to the cation.

Only weak new bands appear in the normally very strong CH out-of-plane bending region between about 900 and 600 cm^{-1} . Most of the detectable new bands fall between 1570 and 1250 cm^{-1} and, thus, are assigned principally to the CC stretching and CH in-plane bending modes of the phenanthrene cation. There undoubtedly are other cation bands that are screened by neutral features. Due to unavoidable confusion from H_2O contamination in the matrix, it is difficult to establish the presence or absence of ion peaks in the 1600 cm^{-1} region from this data.

The cation frequency spectrum, with bands between 1570 and 580 cm^{-1} , resembles that of the neutral species in that the spectrum of neutral phenanthrene is richest between 1600 and 700 cm^{-1} . However, the intensity pattern is remarkably different, a characteristic of all PAH cations studied to date. While neutral phenanthrene has moderate to strong bands between 1600 and 850 cm^{-1} and two very strong bands at about 813 and 735 cm^{-1} (out-of-plane CH bends), the cation band

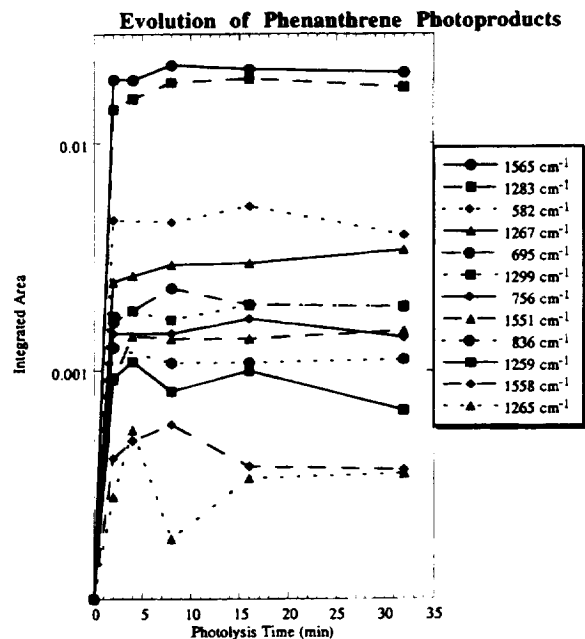


Figure 5. Growth of phenanthrene integrated photoproduct band areas as a function of photolysis time.

intensity pattern is just the opposite, with the bands in the CC stretching and CH in-plane bending region being stronger than those in the CH out-of-plane bending region. Interestingly, the strongest cation bands fall at 1565 and 1277 cm^{-1} , frequencies within the envelopes of the strongest interstellar emission features.

Two cation bands are discernible in the normal CH out-of-plane bending region between 900 and 680 cm^{-1} , namely, those at 836.0 and 756.2 cm^{-1} . They fall close to the regions expected for two and four adjacent hydrogen atoms per aromatic ring, respectively, the types of peripheral H atoms on phenanthrene. Note that both bands (836.0 and 756.2 cm^{-1}) are shifted to higher frequencies by 15–20 cm^{-1} from the very intense bands corresponding to the CH out-of-plane bending vibrations in the neutral molecule (813 and 735 cm^{-1}). Furthermore, one can estimate the intensity of these features relative to those of the neutral molecule. Let n^0 be the number of neutral molecules in the (prephotolysis) sample. n^+ is the number of ions produced by photolysis. The ionization fraction, $I (=n^+/n^0)$, has been measured directly as 0.09 ± 0.04 ($9 \pm 4\%$) by the fractional decrease in the neutral band areas with photolysis for this experiment. The integrated intensities ($\int \tau \nu \equiv a$) of the bands from the CH out-of-plane bending modes of the n^0 neutral phenanthrene molecules are $(a_{813})^0 = 0.165 \text{ cm}^{-1}$ and $(a_{735})^0 = 0.249 \text{ cm}^{-1}$. If the absorption strengths of the CH out-of-plane bends in the ion were the same as those of the neutral molecule, we would expect to see the growth of ion bands with integrated intensities $9 \pm 4\%$ those of the prephotolysis neutral bands or $(a_{836})^+ = (0.09)(0.1647) = 1.5 \times 10^{-2} \text{ cm}^{-1}$ and $(a_{756})^+ = (0.09)(0.2493) = 2.2 \times 10^{-2} \text{ cm}^{-1}$. In reality, the intensities of the 836 and 756 cm^{-1} ion bands are measured to be $(a_{836})^+ = 1.123 \times 10^{-3} \text{ cm}^{-1}$ and $(a_{756})^+ = 1.406 \times 10^{-3} \text{ cm}^{-1}$, respectively, or 13 \times and 16 \times weaker, on average, than those in the neutral molecule. This is in general agreement with our previous results for the naphthalene molecule, where the CH out-of-plane mode was found to be suppressed by a factor of 18 in the cation.

The two bands at 694.5 and 582 cm^{-1} probably arise from CCC plane bending motions.

The Perdeuterated Phenanthrene Cation, $\text{C}_{14}\text{D}_{10}^+$. The mid-infrared spectrum of the fully deuterated phenanthrene cation

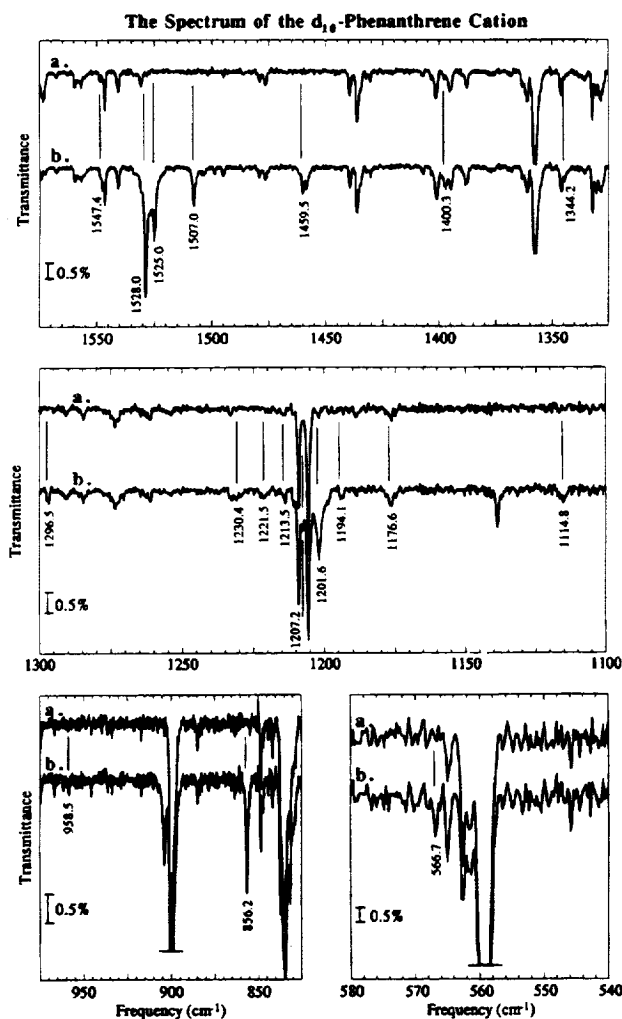


Figure 6. Mid-infrared bands of the perdeuterated phenanthrene cation isolated in an argon matrix at 10 K: (a) before photolysis; (b) after 8 min of *in situ* photolysis. The cation bands are labeled with their positions. Due to its low intensity and separation from other features, the cation band at 1013.4 cm^{-1} is not shown.

is shown in Figure 6. The evolution of the bands assigned to the cation with Lyman- α photolysis is plotted in Figure 7. These bands, together with the corresponding hydrogenated ion bands, are listed in Table 2.

Comparisons between the spectra of the hydrogenated and deuterated PAHs have been used to shed light on the nature of a particular band.^{19,27,32,33} For phenanthrene, however, without the benefit of calculations that take molecular symmetry into account, this technique alone is of rather limited use. The 1565, 1558.2, 1551, and 1513 cm^{-1} bands all fall in the CC stretching region, with a $\nu_{\text{CC}}^{\text{H}}/\nu_{\text{CC}}^{\text{D}}$ ratio of 1.01–1.03 to their presumed deuterated counterparts at 1547.4, 1528/1525, 1507, and 1459.5 cm^{-1} . This assignment to CC stretching modes does not require deuteration.

While the positions of the bands in the 1300–1260 cm^{-1} region of perhydrophenanthrene are suggestive of CC stretching vibrations, it is conceivable that they might have some CH in-plane bend character as well. Simply taking the bands between 1300 and 1250 cm^{-1} and comparing them to the frequencies of the perdeuterated molecule between 1296.5 and 1201 cm^{-1} , one obtains $\nu^{\text{H}}/\nu^{\text{D}}$ ratios in the 1–1.05 range, again consistent with modes that are primarily CC stretching in nature. The difficulty here is that bands also appear upon deuteration between 1194.1 and 856.2 cm^{-1} , suggesting that there are active modes in the hydrogenated species corresponding to CH in-plane bends. By

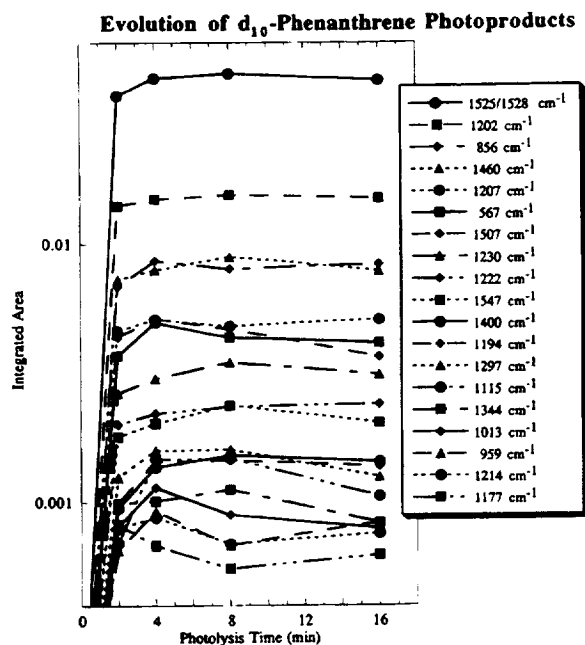


Figure 7. Growth of perdeuterated phenanthrene integrated photo-product band areas as a function of photolysis time.

assuming a $\nu^{\text{H}}/\nu^{\text{D}}$ ratio of 1.15, this would predict CH in-plane bands between about 1370 and 980 cm^{-1} , encompassing the bands between 1300 and 1250 cm^{-1} . As the spectrum of neutral phenanthrene has several absorptions in this region, it is plausible that the corresponding cation bands are screened. It has also been demonstrated that surprisingly large changes in intensity in a given vibrational mode can result from deuteration.^{19,27,32,33} Thus, it may also be that the features observed in this region for the perdeuterated cation are too weak to be visible in the fully hydrogenated cation. It is clear that deuteration alone is not sufficient to make band assignments in the larger PAH molecules.

The Pyrene Cation, $\text{C}_{16}\text{H}_{10}^+$. The mid-infrared absorption bands of the pyrene cation are shown in Figure 8. The cation band frequencies and relative intensities are listed in Table 1. These compare favorably with those reported by Vala et al. for this species.²⁷ We have also observed seven additional bands attributable to the pyrene cation. These bands lie at frequencies of 1556.0, 1356.1, 1255.7, 1253.7, 1188.7, 953.8, and 867.0 cm^{-1} . The bands at 1255.7/1253.7, 1188.7, 953.8, and 867.0 cm^{-1} are weaker than those previously reported, while the bands at 1556.0, and 1356.1 cm^{-1} overlap with previously reported bands and may arise through site effects.

The mid-infrared spectrum is characterized by moderate to strong bands that are rather evenly distributed between 1600 and 600 cm^{-1} . Of the twelve bands between 1600 and 1200 cm^{-1} , the CC stretching region, three are very strong. We have detected two bands in the CH in-plane bend region, at 1102 and 976 cm^{-1} .

The 861 cm^{-1} frequency of the detected out-of-plane CH bend is interesting. Pyrene has two rings with three adjacent H atoms and two rings with two adjacent H atoms. The 861 cm^{-1} band falls at the high limit of the normal range expected for two adjacent H atoms. As the 690 cm^{-1} band falls nearly 60 cm^{-1} below the range for neutral PAHs with three adjacent H atoms on a ring, it is attributed to a CCC bend. Apparently, due to either screening or the inherent weakness of the feature, the absorption corresponding to the triply adjacent CH out-of-plane bend remains undetected. Using an analysis similar to that presented for the phenanthrene cation, we find that the integrated

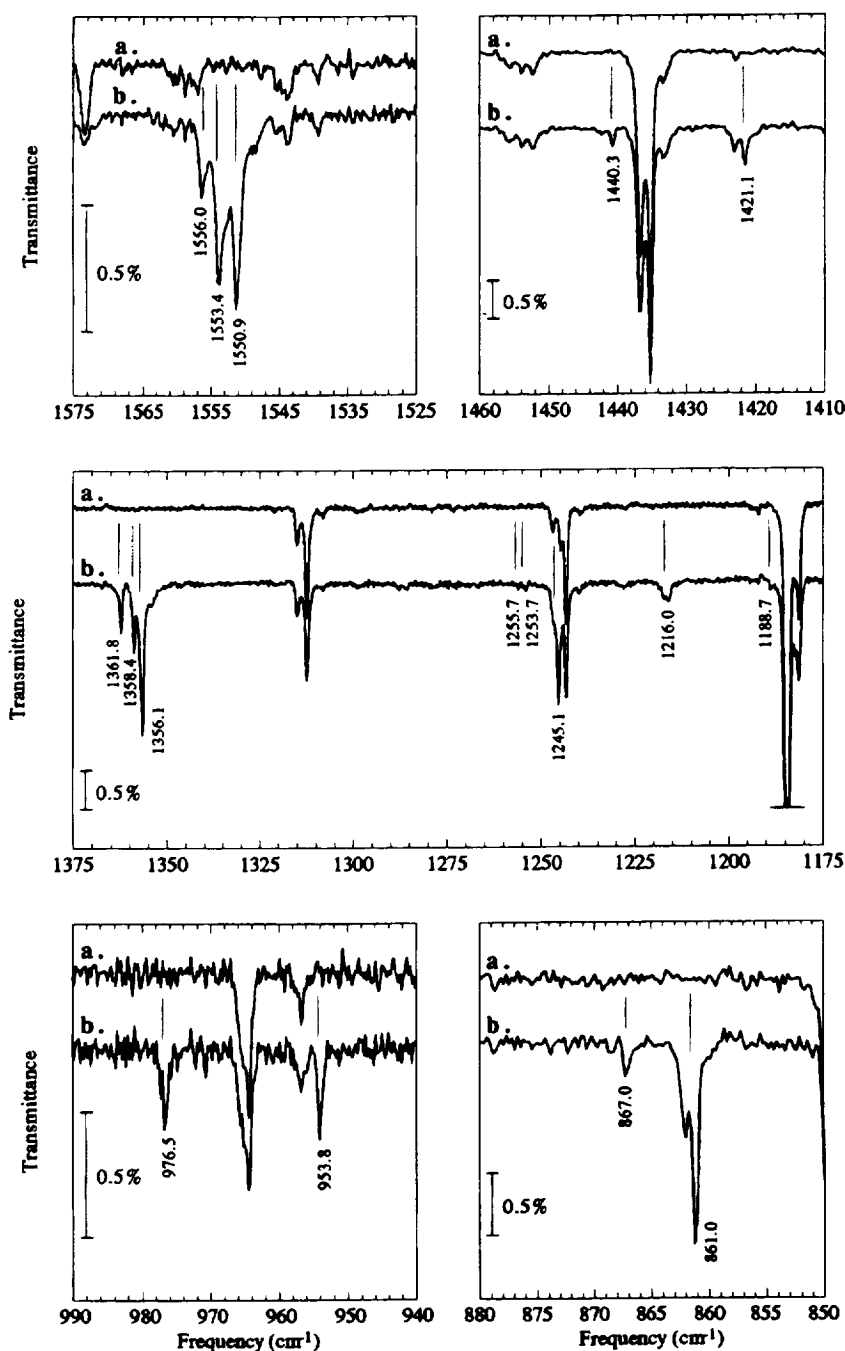


Figure 8. Mid-infrared spectra of the pyrene cation isolated in an argon matrix at 10 K: (a) before photolysis; (b) after 8 min of *in situ* photolysis. The cation bands are labeled with their positions. Due to its low intensity and separation from other features, the cation band at 1102.0 cm^{-1} is not shown.

intensity of the doubly adjacent CH out-of-plane bending mode in the pyrene cation is reduced by a factor of 5 relative to the neutral molecule.

The Perdeuterated Pyrene Cation, $\text{C}_{16}\text{D}_{10}^+$. The mid-infrared spectrum of the fully deuterated pyrene cation is shown in Figure 9. These bands, together with the corresponding hydrogenated ion bands, are also listed in Table 2. The frequencies and assignments are discussed in depth by Vala et al.²⁷ We have found five additional bands attributable to the perdeuterated pyrene cation. These lie at frequencies of 1540.1, 1521.1, 1366.4, 1288.0, and 952.5 cm^{-1} .

The Benzo[e]pyrene Cation, $\text{C}_{20}\text{H}_{12}^+$. The mid-infrared absorption spectrum of the benzo[e]pyrene cation is shown in Figure 10. The cation band frequencies and relative intensities are listed in Table 1. The evolution of the bands assigned to

$\text{C}_{20}\text{H}_{12}^+$ with Lyman- α photolysis is plotted in Figure 11. As with the phenanthrene cation, although this band correlation is looser for the weaker bands, the overall behavior of a sharp rise and leveling off warrants their assignment to the cation. The lines plotted without data points present the behavior of two photoproduct bands not associated with the benzo[e]pyrene cation.

The 11 cation bands in the 1600–1150 cm^{-1} range are dominated by a very strong band at 1349.2 cm^{-1} . All of these bands are attributed to CC stretches. As with perprotonated phenanthrene, no cation features were detected between 1200 and 900 cm^{-1} (the CH in-plane bending region), presumably due to screening by absorptions from the neutral species.

There are two cation bands in the CH out-of-plane bending region. Three are expected since there are three different classes

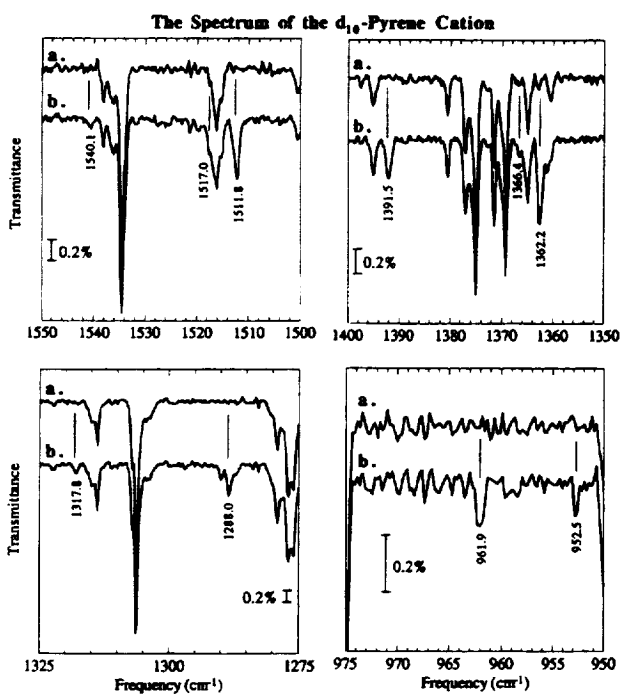


Figure 9. Mid-infrared bands of the perdeuterated pyrene cation isolated in an argon matrix at 10 K: (a) before photolysis; (b) after 8 min of *in situ* photolysis. The cation bands are labeled with their positions.

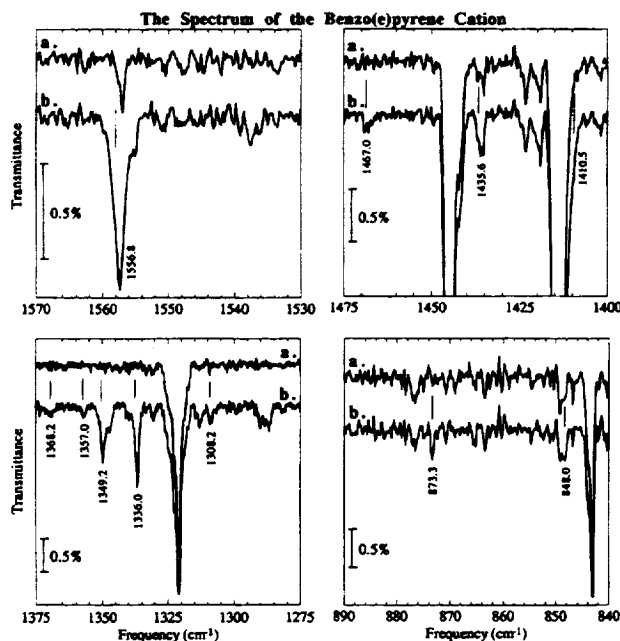


Figure 10. Mid-infrared spectra of the benzo[e]pyrene cation isolated in an argon matrix at 10 K: (a) before photolysis; (b) after 8 min of *in situ* photolysis. The cation bands are labeled with their positions. Bands at 685.7, 1193.9, and 1264.3 cm^{-1} are not shown.

of adjacent hydrogen atoms in this molecule. Benzo[e]pyrene contains one ring with four adjacent H atoms, one ring with two adjacent H's, and two rings with three adjacent H's. The frequencies of the cation bands detected do not fall in the ranges normally attributed to these types of adjacent hydrogen atoms. That at 873.3 cm^{-1} falls several cm^{-1} beyond the high-frequency limit of the range normally attributed to aromatic rings containing two adjacent H atoms, and that at 848.0 cm^{-1} falls within the range for two adjacent H atoms but more than 40 cm^{-1} above that for three. Unless there are important bands in this

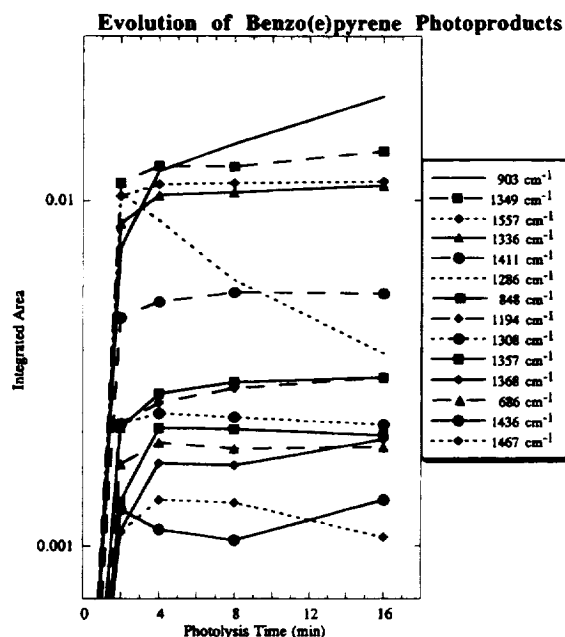


Figure 11. Growth of benzo[e]pyrene integrated photoproduct band areas as a function of photolysis time. Lines with data points indicate bands attributed to the benzo[e]pyrene cation. For comparison, the evolutionary behavior of two photoproduct bands not associated with the PAH cation are also shown (without data points). To avoid confusion among the lowest intensity bands, cation bands at 873.3 and 1264.3 cm^{-1} are not shown.

region screened by the stronger neutral absorptions, these results indicate that the force field for the cation is sufficiently different that these out-of-plane motions not only are reduced dramatically in intensity but that the bond strengths and interactions are altered as well. If the 873.3 cm^{-1} band does indeed arise from the doubly adjacent CH out-of-plane bending vibration, its intensity is suppressed by a factor of 9 from that of the neutral molecule. Furthermore, if the 848 cm^{-1} band arises from the triply adjacent mode, it is remarkable both for its large blue shift from the neutral position ($\nu = 772 \text{ cm}^{-1}$, $\Delta\nu = 76 \text{ cm}^{-1}$) and for the fact that it is only suppressed by a factor of 2 relative to the neutral, much less than the 10–20 \times reduction typically observed in other PAHs.

The band at 685.7 cm^{-1} is assigned to a CCC out-of-plane bend since, in contrast to the other ion CH out-of-plane bending bands, it falls 62 cm^{-1} lower in frequency than the lowest frequency, strong neutral band and about 40 cm^{-1} below the region normally associated with four adjacent H atoms, in the range normally associated with five adjacent H atoms.

The Benzo[ghi]perylene Cation, $\text{C}_{22}\text{H}_{12}^+$. The mid-infrared absorption bands of the benzo[ghi]perylene cation are shown in Figure 12. The cation band frequencies and relative intensities are listed in Table 1. The evolution of the bands assigned to $\text{C}_{22}\text{H}_{12}^+$ with Lyman- α photolysis is plotted in Figure 13. The two lines plotted without data points present the behavior of two photoproduct bands not associated with the benzo[ghi]perylene cation.

Although the benzo[ghi]perylene cation spectrum is similar to that of the benzo[e]pyrene cation in that it is rich in the 1600–1200 cm^{-1} range, it has a very different intensity pattern. This spectrum is dominated by four strong bands in a grouping, which is similar to that found for the interstellar emission spectrum, rather than by one strong band. The strongest band falls at 1578 cm^{-1} , followed by a gap of nearly 200 cm^{-1} , at which point three bands become important, namely, those at 1401.3, 1369, and 1324.4 cm^{-1} . As with phenanthrene and benzo[e]pyrene,

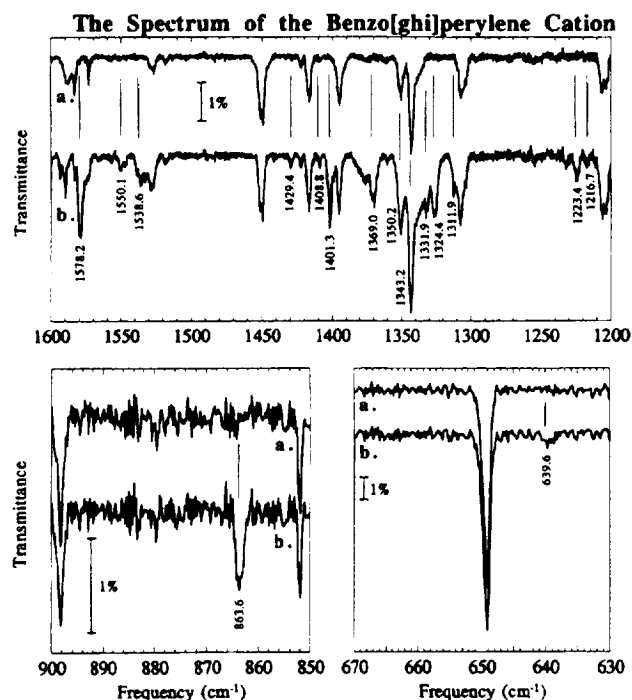


Figure 12. Mid-infrared spectra of the benzo[ghi]perylene cation isolated in an argon matrix at 10 K: (a) before photolysis; (b) after 8 min of *in situ* photolysis. The cation bands are labeled with their positions.

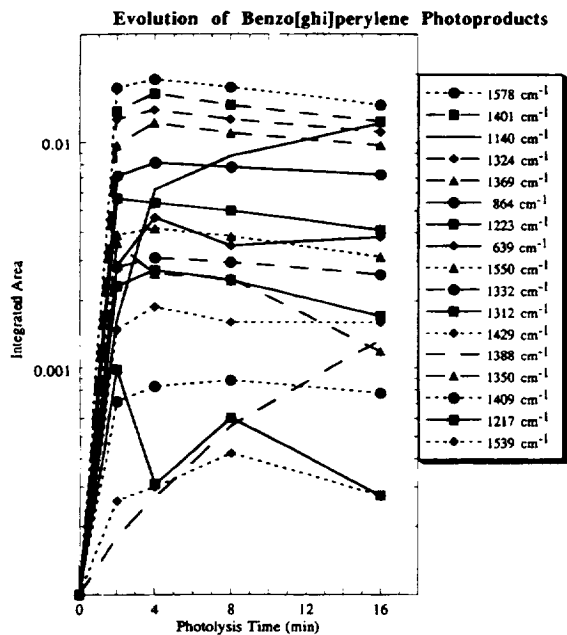


Figure 13. Growth of benzo[ghi]perylene integrated photoproduct band areas as a function of photolysis time. Lines with data points indicate bands attributed to the benzo[ghi]perylene cation. For comparison, the evolutionary behavior of two photoproduct bands not associated with the PAH cation are also shown (without data points).

no cation features were detected between 1200 and 900 cm^{-1} , the CH in-plane bending region. This is puzzling as the spectrum of neutral benzo[ghi]perylene is quite simple in this region, and screening by neutral PAH bands is unlikely.

Only one band, that at 863.6 cm^{-1} , has been detected in the CH out-of-plane bending region of benzo[ghi]perylene. This molecule has two rings with three adjacent H atoms and three rings with two adjacent H's. This band does not fall in the range attributed to doubly adjacent hydrogen, but falls several

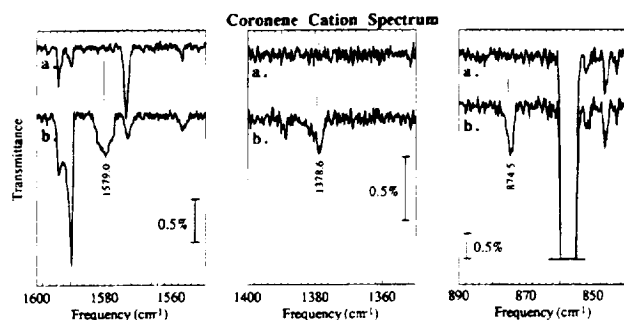


Figure 14. Mid-infrared spectra of the coronene cation isolated in an argon matrix at 10 K: (a) before photolysis; (b) after 8 min of *in situ* photolysis. The cation bands are labeled with their positions.

cm^{-1} beyond the high-frequency limit. Thus, as with the benzo[e]pyrene case, unless there are important bands in this region screened by the stronger neutral absorptions, these results indicate that the force field for the cation is quite different from that of the neutral molecule. As a doubly adjacent CH out-of-plane bend, the intensity of this band is suppressed by a factor of 4 from that of the 846 cm^{-1} band of the neutral molecule.

The band at 639.6 cm^{-1} is assigned to a CCC out-of-plane bend as it is more than 100 cm^{-1} below the region normally associated with three adjacent H atoms, and is even well out of the range associated with five adjacent H atoms.

The Coronene Cation, $\text{C}_{24}\text{H}_{12}^+$. The mid-infrared absorption bands of the coronene cation are shown in Figure 14. The cation band frequencies and relative intensities are listed in Table 1. The positions and relative intensities of the bands at 1378.6 and 874.5 cm^{-1} agree well with those previously published.^{28b,29} The band at 1579 cm^{-1} has not been reported.

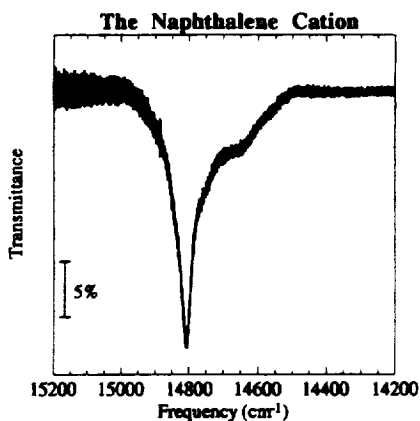
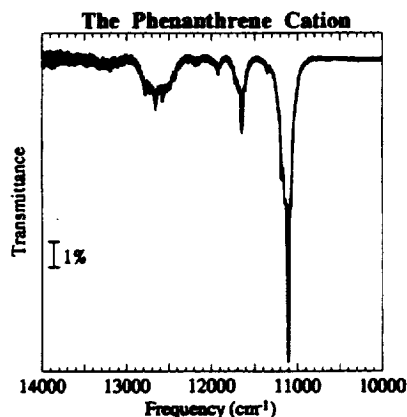
The coronene cation spectrum is remarkable for its simplicity and unusual intensity pattern. Only three cation bands have been reported, and the intensity pattern is opposite those of all other PAH cations studied to date, with the CH out-of-plane bend producing a band slightly stronger than that arising from the CC stretching modes. It should be pointed out that the ionization percentage calculated for this experiment is 11%, comparable to that obtained for the other PAHs in the series. Furthermore, the intensity of the detected CH out-of-plane bending feature is also comparable to that measured for the other cations. Thus, we conclude that the CC stretching modes in the coronene cation are anomalously weak, giving rise to the atypical intensity pattern.

Two bands fall in the CC stretching range (1579 and 1378.6 cm^{-1}), none are in the CH in-plane bend region, and one falls in the CH out-of-plane bend region (874.5 cm^{-1}). These three bands fall at frequencies very close to those of prominent bands in the interstellar emission spectrum. As with benzo[ghi]perylene, it seems odd that no bands were detectable in the CH in-plane bend region, as the spectrum of the neutral species is extremely simple in this area and screening is not a reasonable explanation for the absence of cation bands. High symmetry seems plausible to account for the overall simplicity of the spectrum, the weakness of the CC stretching bands, and the absence of detectable bands in the CH in-plane bend region. The position of the out-of-plane CH bend of the cation is interesting in this regard in that, as with the other PAH cations in this series, it falls on the high side of the normal range expected for two adjacent H atoms and is reduced in intensity by a factor of 5 from that of the 857 cm^{-1} band of neutral coronene.

B. Near-Infrared Spectroscopy. Band frequencies, areas, and relative intensities listed in Table 3 for the near-IR spectra

TABLE 3: Near-Infrared Frequencies and Relative Intensities of Several Cations from the Thermodynamically Most Favored PAHs

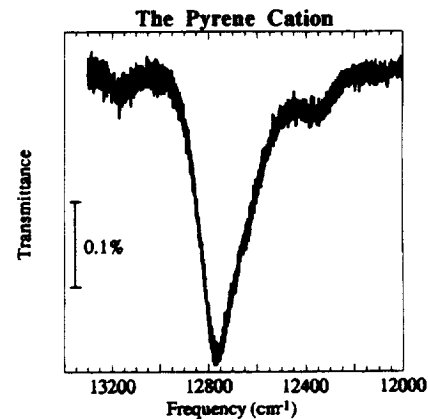
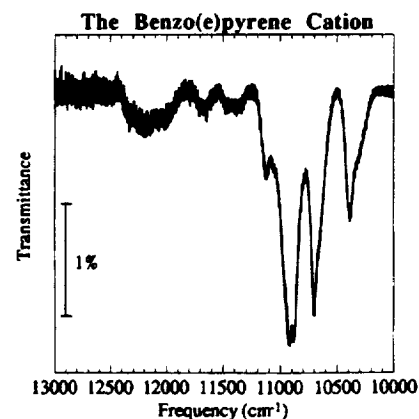
naphthalene		phenanthrene		phenanthrene- <i>d</i> ₁₀		pyrene		benzo[<i>e</i>]pyrene		benzo[<i>ghi</i>]perylene		coronene	
ν (cm ⁻¹)	<i>I</i> _{rel}	ν (cm ⁻¹)	<i>I</i> _{rel}	ν (cm ⁻¹)	<i>I</i> _{rel}	ν (cm ⁻¹)	<i>I</i> _{rel}	ν (cm ⁻¹)	<i>I</i> _{rel}	ν (cm ⁻¹)	<i>I</i> _{rel}	ν (cm ⁻¹)	<i>I</i> _{rel}
14805	1.00	11105	1.00	11145	1.00	12760	1.00	10373	0.258	12185	0.251	10409	1.00
		11650	0.175	11669	0.185			10687	0.255	12481	0.225	10677	0.170
		12600	0.376	12647	0.436			10892	1.00	13049	1.00	10886	0.324
								12166	0.500	13284	0.113	11170	0.0907
										13444	0.275	11340	0.0239
												11417	0.152
												11610	0.149
												11845	0.100
												11990	0.0719
												12471	0.142
												12766	0.0273

**Figure 15.** Near-infrared spectrum of the naphthalene cation isolated in an argon matrix at 10 K. This is the 0-0 band of the D₂ ← D₀ transition.**Figure 16.** Near-infrared spectrum of the phenanthrene cation isolated in an argon matrix at 10 K. This is the D₂ ← D₀ transition. The strongest band corresponds to the 0-0 transition. The mid-infrared spectrum of the same sample is shown in Figure 4.

were measured on the same matrices for which the mid-IR bands listed in Table 1 were measured.

The Naphthalene Cation, C₁₀H₈⁺. The near-infrared spectrum of the naphthalene cation is shown in Figure 15. The electronic spectrum of this cation has been described in detail previously.^{25,34}

The Phenanthrene Cation, C₁₄H₁₀⁺. The near-infrared spectrum of the phenanthrene cation is shown in Figure 16, with frequencies and relative intensities listed in Table 3. The near-infrared spectrum of the phenanthrene cation isolated in an argon matrix has been discussed by Andrews et al.³⁵ and that in a neon matrix by Salama et al.³⁶ The near-infrared spectrum of the phenanthrene-*d*₁₀ cation is not shown since it resembles that

**Figure 17.** Near-infrared spectrum of the pyrene cation isolated in an argon matrix at 10 K. This is the 0-0 band of the D₂ ← D₀ transition. The mid-infrared spectrum of the same sample is shown in Figure 8 (argon matrix, 10 K).**Figure 18.** Near-infrared spectrum of the benzo[*e*]pyrene cation isolated in an argon matrix at 10 K. This is the D₂ ← D₀ transition. The strongest band corresponds to the 0-0 transition. The mid-infrared spectrum of the same sample is shown in Figure 10.

of perhydrophenanthrene. The frequencies of phenanthrene-*d*₁₀ are listed in Table 2.

The Pyrene Cation, C₁₆H₁₀⁺. The near-infrared spectrum of the pyrene cation is shown in Figure 17, with frequencies and relative intensities listed in Table 3. The near-infrared spectra of the pyrene cation isolated in argon and neon matrices have been described previously.^{27,37}

The Benzo[*e*]pyrene Cation, C₂₀H₁₂⁺. The near-infrared spectrum of the benzo[*e*]pyrene cation is shown in Figure 18, with frequencies and relative intensities listed in Table 3.

The Benzo[*ghi*]perylene Cation, C₂₂H₁₂⁺. The near-infrared spectrum of the benzo[*ghi*]perylene cation is shown in Figure 19, with frequencies and relative intensities listed in Table 3.

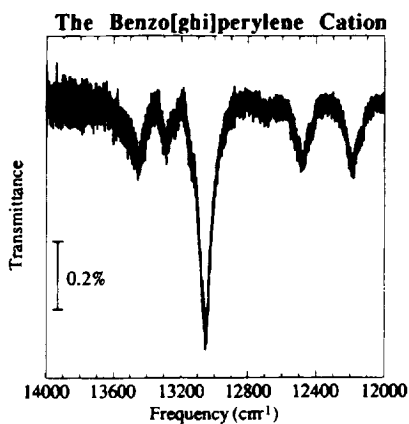


Figure 19. Near-infrared spectrum of the benzo[ghi]perylene cation isolated in an argon matrix at 10 K. This is the $D_2 - D_0$ transition. The strongest band corresponds to the 0-0 transition. The mid-infrared spectrum of the same sample is shown in Figure 12.

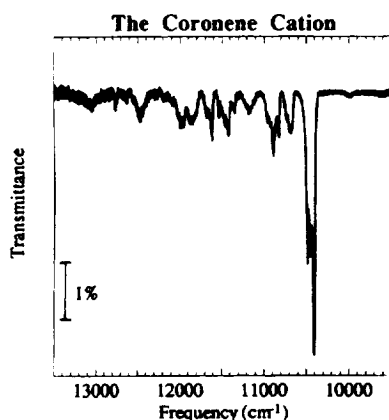


Figure 20. Near-infrared spectrum of the coronene cation isolated in an argon matrix at 10 K. This is the $D_1 - D_0$ transition. The strongest band corresponds to the 0-0 transition. The mid-infrared spectrum of the same sample is shown in Figure 14.

The Coronene Cation, $C_{24}H_{12}^+$. The near-infrared spectrum of the coronene cation is shown in Figure 20, with frequencies and relative intensities listed in Table 3. The near-infrared spectrum of the coronene cation isolated in an argon matrix has been reported by d'Hendecourt et al.²⁹

C. Integrated Absorbance Values. Integrated absorbance values [A (kilometers/mole)] for the mid-infrared cation bands of the PAHs phenanthrene, pyrene, benzo[ghi]perylene, and coronene are listed in Table 4. These A -values were determined using the near-infrared spectra presented earlier in the following way.

The integrated absorbance value, A , is given by the relation

$$A = \int \tau \, d\nu / N^+ \quad (1)$$

where N^+ is the number density of absorbers, in this case PAH cations, and $\int \tau \, d\nu$ is the integrated area of the strongest near-infrared band (in centimeters⁻¹). N^+ (in moles centimeters⁻²) is related to the area of this band by the equation

$$N^+ = \tau \Delta\nu / \epsilon_{\max}^+ \Delta\nu \quad (2)$$

where $\epsilon_{\max}^+ \Delta\nu$ is the integrated molar absorption coefficient in liters mole⁻¹. Combination of eqs 1 and 2 gives

$$A_{\text{NIR}} = \epsilon_{\max}^+ \Delta\nu \quad (3)$$

where $\Delta\nu$ is the measured full width at half-height (FWHH) of

the near-infrared band, and the value of the molar absorption coefficient ϵ_{\max}^+ was determined from the oscillator strength (f) using³⁸

$$n_{\text{Ar}}^f = 4.32 \times 10^{-9} \epsilon_{\max}^+ \Delta\nu \quad (n_{\text{Ar}} = 1.29) \quad (4)$$

A straightforward unitary conversion gives the integrated absorbance value in units of kilometers/mole. The ratio of the integrated area of the mid-infrared bands to that of the near-infrared band *in the same matrix* could then be used to scale A_{NIR} , giving the integrated absorbance values presented in Table 4. All integrated band areas were calculated in base 10 with software provided by Nicolet. The specific oscillator strengths, molar absorption coefficients, and near-IR/mid-IR band ratios used for our calculations are given in the following.

It should also be emphasized that our experiments indicate that the presence of CCl_4 significantly *enhances* the near-infrared band intensities with respect to the mid-infrared band intensities. For example, without CCl_4 in the matrix, the ratio of the integrated intensity of the 9005 Å phenanthrene electronic band to the 1565 cm^{-1} vibrational band is 66. With CCl_4 , the ratio is 139. The presence of CCl_4 enhances the ratio by about 2 times. For benzo[e]pyrene, without CCl_4 in the matrix, the ratio of the integrated intensity of the 9181 Å electronic band to the 1349.2 cm^{-1} vibrational band is 43. With CCl_4 , the ratio is 59, an enhancement of about 40%. For the 7663 Å and 1401.3 cm^{-1} bands of benzo[ghi]perylene, the enhancement is about 6 times ($\int \tau \, d\nu_{\text{NIR}} / \int \tau \, d\nu_{\text{MIR}} = 9$ without CCl_4 and 55 with CCl_4). In ref 19, we showed that CCl_4 did not influence the absolute strength of naphthalene's mid-infrared bands, but did not investigate its influence on any electronic transitions.

In view of the near- to mid-infrared intensity ratio alterations induced by CCl_4 , A -values were determined for matrices *without* CCl_4 present. Ultimately, the accuracy of these values rests on the molar absorption coefficient used to determine the number of neutral PAH molecules lost upon photolysis, the technique generally used to determine the molar absorption coefficients and oscillator strengths of the near-infrared cation bands.³⁶ As this information is not available for all of the PAHs studied here, we have been unable to determine A -values for all the cations reported. The integrated A -values for the other PAH cation bands will be evaluated as this information becomes available.

This is an extremely important issue as there is wide variance in the literature on this subject. As with the naphthalene cation, and as discussed at length in ref 19, while the *relative* intensities of the cation bands reported here agree well in those cases where independently measured data are available (pyrene and coronene), there are discrepancies between the reported *absolute* intensities. However, while discrepancies still exist between our results and those from Professor Vala's group at the University of Florida, they are much more modest than was the case for the naphthalene cation (2-4× as compared to 50×). Such variances may well be within the experimental uncertainties associated with the measurements, conservatively estimated to be less than a factor of 2. By far the largest source of error in these measurements stems from the lack of accurate molar absorbances for the near-IR bands. In order to reduce the relative uncertainty in these values, and to eliminate the possibility of matrix effects influencing the electronic transitions differently from the vibrational transitions, we are developing an alternative method to determine A -values. In view of the fundamental importance of these values, we present the details of our A -value calculations.

Naphthalene Integrated A-Values. The analysis described earlier was applied to the naphthalene cation in order to check

TABLE 4: Integrated Absorbance Values for the Mid-Infrared Bands of Several PAH Cations^a

phenanthrene				pyrene C ₁₆ H ₁₀ ⁺		benzo[ghi]perylene C ₂₂ H ₁₂ ⁺		coronene C ₂₄ H ₁₂ ⁺	
C ₁₄ H ₁₀ ⁺		C ₁₄ D ₁₀ ⁺		ν (cm ⁻¹)	A (km/mol)	ν (cm ⁻¹)	A (km/mol)	ν (cm ⁻¹)	A (km/mol)
582.00	0.594	566.70	0.424	690.10	64.3	639.60	81.5	874.50	179
694.50	0.255	856.20	0.785	861.00	76.1	863.60	166	1378.6	31.1
756.20	0.197	958.50	0.0769	867.00	9.95	1216.7	11.9	1579.0	148
836.00	0.150	1013.4	0.0899	953.80	18.8	1223.4	110		
1258.7	0.112	1114.8	0.115	976.50	25.5	1311.9	50.1		
1264.7	0.0383	1176.6	0.0676	1102.0	22.4	1324.4	276		
1267.0	0.383	1194.1	0.130	1188.7	10.3	1331.9	62.8		
1277.5/1282.5	2.26	1201.6	1.47	1216.0	34.1	1343.2	120		
1299.0	0.239	1207.2	0.487	1245.1	96.7	1350.2	53.5		
1513.0	0.114	1213.5	0.0781	1253.7/1255.7	12.0	1369.0	234		
1551.0	0.169	1221.5	0.223	1356.1/1358.4	282	1401.3	312		
1558.2	0.0570	1230.4	0.303	1361.8	44.6	1408.8	17.7		
1565.0	2.70	1296.5	0.141	1421.1	44.6	1429.4	36.3		
		1344.2	0.0983	1440.3	28.5	1538.6	6.92		
		1400.3	0.130	1550.9/1553.4/1556.0	251	1550.1	82.3		
		1459.5	0.794			1578.2	374		
		1507.0	0.441						
		1525.0/1528.0	4.20						
		1547.4	0.204						

^a Experimental uncertainties of the integrated absorbance values are less than a factor of 2.

the technique. We had previously derived the naphthalene cation *A*-values using an entirely independent analysis.¹⁹ Use of the amended molar absorption coefficient for the 6754 Å band of the naphthalene cation,¹⁹ $\epsilon_{\max}^+ = 565 \text{ L mol}^{-1} \text{ cm}^{-1}$, and FWHH = 45 cm⁻¹ in eq 3 gives $A_{\text{NIR}} = 254 \text{ km/mol}$. The ratio of the 1218 cm⁻¹ band of the naphthalene cation, the strongest mid-infrared feature, to the 6750 Å band measured for this experiment is 1/65, giving an *A*-value for this band of $A_{1218} = 3.9 \text{ km/mol}$. This is in excellent agreement with the value of 4.1 km/mol presented in ref 19, supporting the validity of this technique.

Phenanthrene Integrated *A*-Values. The oscillator strength for the 9005 Å band of phenanthrene is 6×10^{-5} .³⁶ Use of eq 4 and a 53 cm⁻¹ FWHH gives $\epsilon_{\max}^+ = 338 \text{ L mol}^{-1} \text{ cm}^{-1}$. Equation 3 gives $A_{\text{NIR}} = 1.79 \times 10^2 \text{ km/mol}$. Finally, the ratio of the strongest mid-infrared band, 1565 cm⁻¹, to the 9005 Å near-infrared band is 1/66, giving $A_{1565} = 2.7 \text{ km/mol}$. The other mid-infrared *A*-values were scaled using the relative intensities shown in Table 1.

Phenanthrene-*d*₁₀ Integrated *A*-Values. The oscillator strength for the 8973 Å band of phenanthrene-*d*₁₀ is assumed equal to that for phenanthrene, i.e., 6×10^{-5} .³⁶ This gives $\epsilon_{\max}^+ = 188 \text{ L mol}^{-1} \text{ cm}^{-1}$ (FWHH = 95 cm⁻¹) and $A_{\text{NIR}} = 179 \text{ km/mol}$. The ratio of the 1528 cm⁻¹ mid-infrared band to the 8973 Å band in phenanthrene-*d*₁₀ is 1/42, giving $A_{1528} = 4.2 \text{ km/mol}$. The other mid-infrared *A*-values were scaled using the relative intensities shown in Table 2.

Pyrene Integrated *A*-Values. The oscillator strength for the 7837 Å band of pyrene is assumed to be about 1×10^{-3} .³⁹ This gives $\epsilon_{\max}^+ = 1420 \text{ L mol}^{-1} \text{ cm}^{-1}$ (FWHH = 210 cm⁻¹) and $A_{\text{NIR}} = 2.99 \times 10^3 \text{ km/mol}$. The ratio of the 1356.1 cm⁻¹ mid-infrared band to the 7837 Å band of pyrene is 1/11, giving $A_{1356} = 282 \text{ km/mol}$. The other mid-infrared *A*-values were scaled using the relative intensities shown in Table 1.

Benzo[ghi]perylene Integrated *A*-Values. The oscillator strength for the 7663 Å band of benzo[ghi]perylene is also taken as 1×10^{-3} .³⁹ This corresponds to $\epsilon_{\max}^+ = 3830 \text{ L mol}^{-1} \text{ cm}^{-1}$, based on a 78 cm⁻¹ FWHH. The integrated absorbance value is $A_{\text{NIR}} = 2.99 \times 10^3 \text{ km/mol}$. The ratio of the 1578.2 cm⁻¹ mid-infrared band to the 7663 Å band of benzo[ghi]-

perylene is 1/8, giving $A_{1578} = 374 \text{ km/mol}$. The other mid-infrared *A*-values were scaled using the relative intensities shown in Table 1.

Coronene Integrated *A*-Values. The oscillator strength for the 9607 Å band of coronene is 1.8×10^{-3} .⁴⁰ This corresponds to $\epsilon_{\max}^+ = 5.84 \times 10^3 \text{ L mol}^{-1} \text{ cm}^{-1}$, based on a 92 cm⁻¹ FWHH. This, in turn, gives $A_{\text{NIR}} = 5.38 \times 10^3 \text{ km/mol}$. The ratio of the 874.5 cm⁻¹ mid-infrared band to the 9607 Å band of coronene is 1/30, giving $A_{875} = 179 \text{ km/mol}$. The other mid-infrared *A*-values were scaled using the relative intensities shown in Table 1.

IV. Astrophysical Implications

Comparisons between the interstellar emission spectra and the absorption spectra of PAHs in KBr pellets have shown important differences, which are used by some to draw conclusions about the nature of interstellar PAHs and by others to raise doubts as to the validity of the PAH hypothesis. One important difference concerns relative band intensities. As shown in Figure 21, which presents the IR emission spectrum from the Great Nebula in Orion,⁴¹ the interstellar 1610 cm⁻¹ (6.2 μm) feature and broad emission envelope centered near 1300 cm⁻¹ (7.7 μm), which are assigned to PAH CC stretching modes, are *much* more intense than the interstellar feature near 885 cm⁻¹ (11.3 μm), which is attributed to the CH out-of-plane bending mode. This behavior is just the opposite that of PAHs in KBr pellets and in solvents where the strongest absorptions by far are those due to the out-of-plane CH bending vibrations [often 5–8 times greater than the average band strength in the CC stretch and CH in-plane bending region between about 1650 and 1100 cm⁻¹ (6 and 9 μm)]. The relative intensities of the interstellar features have been taken by some as evidence that interstellar PAHs are severely dehydrogenated, in spite of the fact that atomic hydrogen is on the order of 10 000 times more abundant in most of the emission zones than the PAHs.⁴² To invoke such a high degree of dehydrogenation under these conditions seems unreasonable.

This difficulty is removed if the PAHs in space are largely ionized. With the exception of coronene, we have shown the following: First, the intensities of the bands in the 1650–1100 cm⁻¹ range, the CC stretching and CH in-plane bending region

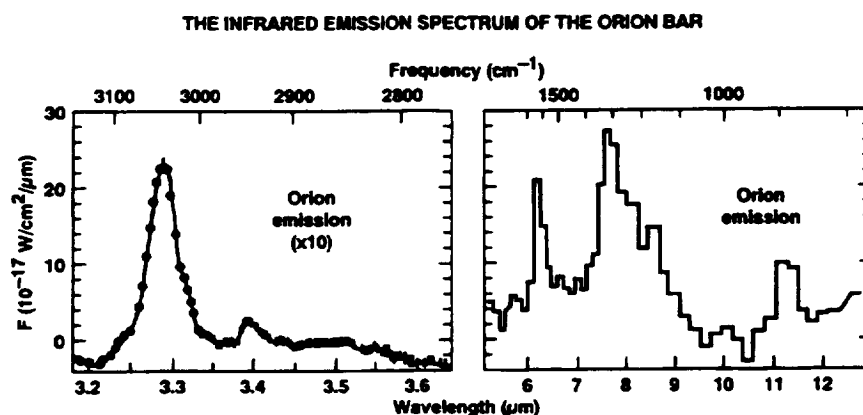


Figure 21. Infrared emission spectrum from the Orion nebula.⁴¹

of PAH cations, are typically 2–5 times greater than those of the CH out-of-plane bending modes, which fall between 900 and 550 cm^{-1} . Second, the CH out-of-plane bending modes of the cations are typically 5–20 times weaker than the out-of-plane bending modes of the neutral molecules, and third, the bands in the the CC stretching and CH in-plane bending regions are generally an order of magnitude stronger than those for the corresponding transitions in neutral PAHs. The coronene exception is notable. The 874.5 cm^{-1} CH out-of-plane bend of the coronene cation is slightly stronger than the strongest CC stretch at 1579 cm^{-1} .

This work and work presented by the University of Florida group on other PAH cations^{25–28} confirm the behavior predicted theoretically by Defrees et al.²³ and Pauzat et al.²⁴ and resolve one of the more troubling aspects of the interstellar PAH model. Other impediments to the full exploitation of the interstellar PAH hypothesis raised by comparing KBr pellet spectra to the interstellar spectra are addressed by the results of a study of the spectroscopic properties of a number of neutral, matrix-isolated PAHs found elsewhere.^{21,22}

It is important to realize that the most intense bands of all PAH cations studied to date fall within the envelopes of the most intense interstellar features, namely, those at 6.2 and 7.7 μm . As illustrated by Figure 21, these are consistently the broadest and most intense members of the interstellar emission band family. The observation that the most intense interstellar emission features fall in the PAH CC stretching and CH in-plane bending regions is completely consistent with the composite emission spectrum expected from a mixture dominated by free, ionized, small PAHs.

V. Conclusions

The near- and mid-infrared spectra of the phenanthrene, pyrene, benzo[e]pyrene, benzo[ghi]perylene, and coronene cations, isolated in argon matrices, are reported. Ions were generated by *in situ* photolysis.

With the exception of coronene, the strongest mid-infrared absorption bands of these PAH cations fall between 1600 and 1200 cm^{-1} , the CC stretching and CH in-plane bending region. These tend to be 2–5 times more intense than the bands due to the CH out-of-plane bending modes. The strongest bands tend to fall in groupings between 1600 and 1550 cm^{-1} and between 1400 and 1200 cm^{-1} .

On the other hand, integrated absorbance values for the CH modes in the cation are strongly depressed with respect to the neutral molecules. Only weak new bands grow in the normally very strong CH out-of-plane bending region between about 900 and 600 cm^{-1} . The extent to which these out-of-plane motions are reduced in intensity and the bond strengths and interactions

are altered is far more than would be expected on first principles by the removal of one electron from the π system. Similarly, as has been the case with previous PAH cations studied, no new features were found in the CH stretching region between 3200 and 2900 cm^{-1} , implying that the CH stretching modes of the cation are comparable to or weaker than those for the neutral species. Theory predicts them to be weaker.²⁴

Most of the detectable new bands fall between 1570 and 1250 cm^{-1} and, thus, are assigned principally to the CC stretching modes. Those at the lower frequencies in this range may have some in-plane CH bending character as well.

The observation that the strongest cation bands coincide with CC stretching modes, behavior just the opposite that of the neutral species, has important ramifications on the interpretation of the observed astronomical emission spectrum, which is dominated by very broad features in this region at 1310 and 1620 cm^{-1} . Since this seems to be a general characteristic of PAH cations, it resolves one of the greatest discrepancies with the interstellar PAH hypothesis.

Acknowledgment. The authors acknowledge the expert technical support of Bob Walker and valuable scientific discussions with Farid Salama, Scott Sandford, and Christine Joblin. This work was fully supported by NASA's Laboratory Astrophysics and Long Term Space Astrophysics programs under Grants 188-44-57-01 and 399-20-01-05.

Note Added in Proof: Recent unpublished calculations on PAH cation integrated absorbance values (*A*-values) by Langhoff show considerable PAH to PAH variation when compared to the values in Table 4. The experimental values tend to be no more than a factor of 2 greater than the theoretical values for pyrene, but they are 2–3 orders of magnitude smaller for phenanthrene. This points out the need for a better understanding of *A*-values in PAH cations.

References and Notes

- (1) Harvey, R. G., Ed. *Polycyclic Hydrocarbons and Carcinogenesis*; American Chemical Society: Washington, DC, 1985.
- (2) (a) Harris, S. J.; Weiner, A. M. *Combust. Sci. Technol.* **1983**, *31*, 155. (b) Frenklach, M.; Wamatz, J. *Combust. Sci. Technol.* **1987**, *51*, 265.
- (3) (a) Allamandola, L. J.; Tielens, A. G. G. M.; Barker, J. R. *Astrophys. J. Suppl. Ser.* **1989**, *71*, 733. (b) Allamandola, L. J. In *Topics in Current Chemistry*; Cyvin, S., Gutman, J., Eds.; Springer Verlag: Berlin, 1990; p 1. (c) Puget, J. L.; Leger, A. *Annu. Rev. Astron. Astrophys.* **1989**, *27*, 161.
- (4) Allamandola, L. J.; Tielens, A. G. G. M.; Barker, J. R. *Astrophys. J. Lett.* **1985**, *290*, L25.
- (5) Leger, A.; Puget, J. L. *Astron. Astrophys.* **1984**, *137*, L5.
- (6) (a) Cyvin, B. N.; Klaeboe, P.; Whitmer, J. C.; Cyvin, S. J. *Z. Naturforschung* **1982**, *37a*, 251. (b) Cyvin, S. J.; Cyvin, B. N.; Brunvoll, J.; Whitmer, J. C.; Klaeboe, P.; Gustavsen, J. E. *Z. Naturforschung* **1979**, *34a*, 876.

- (7) *Sadtler Atlas of Infrared Spectra*; Sadtler Research Laboratories: Philadelphia, PA, 1990.
- (8) Witteborn, F. C.; Sandford, S. A.; Bregman, J. D.; Allamandola, L. J.; Cohen, M.; Wooden, D. H.; Graps, A. L. *Astrophys. J.* **1989**, *341*, 270.
- (9) Cherkneff, I.; Barker, J. R. *Astrophys. J. Lett.* **1989**, *341*, L21.
- (10) Shan, J.; Suto, M.; Lee, L. C. *Astrophys. J.* **1991**, *383*, 459.
- (11) Brenner, J. D.; Barker, J. R. *Astrophys. J. Lett.* **1992**, *388*, L39.
- (12) Schlemmer, S.; Cook, D. J.; Harrison, J. A.; Wurfel, B.; Chapman, W.; Saykally, R. J. *Science* **1994**, *265*, 1686.
- (13) Williams, R. M.; Leone, S. R. In *The Diffuse Interstellar Bands: Contributed Papers*; Tielens, A. G. G. M., Ed.; NASA: Washington, DC, 1994; CP 10144, p 59.
- (14) Flickinger, G. C.; Wdowiak, T. J.; Gomez, P. L. *Astrophys. J. Lett.* **1991**, *380*, L43.
- (15) Colangeli, L.; Mennella, V.; Bussoletti, E. *Astrophys. J.* **1992**, *385*, 577.
- (16) Kurtz, J. *Astron. Astrophys.* **1992**, *255*, L1.
- (17) Joblin, C.; Boissel, P.; Leger, A.; d'Hendecourt, L. B.; Defourneau, D. *Astron. Astrophys. J.* **1994**, in press.
- (18) Wdowiak, T. J., 1994, private communication.
- (19) Hudgins, D. M.; Sandford, S. A.; Allamandola, L. J. *J. Phys. Chem.* **1994**, *98*, 4243.
- (20) Stein, S. E. *J. Phys. Chem.* **1978**, *82*, 270.
- (21) Hudgins, D. M.; Sandford, S. A. manuscript in preparation.
- (22) Hudgins, D. M.; Sandford, S. A., manuscript in preparation.
- (23) (a) DeFrees, D. J.; Miller, M. D. In *Interstellar Dust: Contributed Papers*; Allamandola, L. J.; Tielens, A. G. G. M., Eds.; NASA: Washington, DC, 1989; CP 3036, p 173. (b) DeFrees, D. J.; Miller, M. D.; Talbi, D.; Pauzat, F.; Ellinger, Y. *Astrophys. J.* **1993**, *408*, 530.
- (24) Pauzat, F.; Talbi, D.; Miller, M. D.; DeFrees, D. J.; Ellinger, Y. *J. Phys. Chem.* **1992**, *96*, 7882.
- (25) Szczepanski, J.; Roser, D.; Personette, W.; Eyring, M.; Pellow, R.; Vala, M. *J. Phys. Chem.* **1992**, *96*, 7876.
- (26) Szczepanski, J.; Vala, M.; Talbi, D.; Parisel, O.; Ellinger, Y. *J. Chem. Phys.* **1993**, *98*, 4494.
- (27) Vala, M.; Szczepanski, J.; Pauzat, F.; Parisel, O.; Talbi, D.; Ellinger, Y. *J. Phys. Chem.* **1994**, *98*, 9187-9196.
- (28) Szczepanski, J.; Chapiro, C.; and Vala, M. *Chem. Phys.* **1993**, *205*, 434. (b) Szczepanski, J.; Vala, M. *Astrophys. J.* **1993**, *414*, 179.
- (29) d'Hendecourt, L. B.; Leger, A. In *The First Symposium on the Infrared Cirrus and Diffuse Interstellar Clouds, ASP Conference Series Vol. 58*; Cutri, R. M., Latter, W. B., Eds.; Astronomical Society of the Pacific: San Francisco, 1994.
- (30) White, C. M. *J. Chem. Eng. Data* **1986**, *31*, 198.
- (31) Werner, A. S.; Tsai, B. P.; Baer, T. *J. Chem. Phys.* **1974**, *60*, 3650.
- (32) Lippincott, E. R.; O'Reilly, E. J. *J. Chem. Phys.* **1955**, *23*, 238.
- (33) McClellan, A. L.; Pimentel, G. C. *J. Chem. Phys.* **1955**, *23*, 245.
- (34) Salama, F.; Allamandola, L. J. *J. Chem. Phys.* **1991**, *94*, 6964.
- (35) Andrews, L.; Friedman, S.; Kelsall, J. *J. Phys. Chem.* **1985**, *89*, 4016.
- (36) Salama, F.; Joblin, C.; Allamandola, L. J. *J. Chem. Phys.* **1994**, *101*, 10252.
- (37) Salama, F.; Allamandola, L. J. *Nature* **1992**, *358*, 42.
- (38) Okabe, H. *Photochemistry of Small Molecules*; Wiley & Sons: New York, 1978; p 41.
- (39) Salama, F., private communication.
- (40) Ehrenfreund, P.; d'Hendecourt, L.; Verstraete, L.; Leger, A.; Schmidt, W.; Defourneau, D. *Astron. Astrophys.* **1992**, *259*, 257.
- (41) Bregman, J. D.; Allamandola, L. J.; Tielens, A. G. G. M.; Geballe, T. R.; Witteborn, F. C. *Astrophys. J.* **1989**, *344*, 791.
- (42) Jourdain de Muizon, M.; d'Hendecourt, L. B., and Geballe, T. R., *Astron. Astrophys.*, **1990**, *227*, 526.

JP942323L